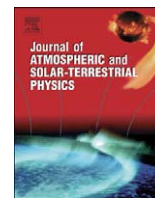




Contents lists available at ScienceDirect

Journal of Atmospheric and Solar-Terrestrial Physics

journal homepage: www.elsevier.com/locate/jastp

Seasonal and diurnal variability of the meteor flux at high latitudes observed using PFISR

J.J. Sparks^{a,b}, D. Janches^{a,*}, M.J. Nicolls^c, C.J. Heinselman^c^a NorthWest Research Associates, CoRA Division, Boulder, CO, USA^b Department of Physics, University of Colorado, Boulder, CO, USA^c SRI International, Menlo Park, CA, USA

ARTICLE INFO

Article history:

Accepted 21 August 2008

Available online 10 September 2008

Keywords:

Meteors

Radar

Head-echo

MLT

PFISR

ABSTRACT

We report in this and a companion paper [Fentzke, J.T., Janches, D., Sparks, J.J., 2008. Latitudinal and seasonal variability of the micrometeor input function: A study using model predictions and observations from Arecibo and PFISR. *Journal of Atmospheric and Solar-Terrestrial Physics*, this issue, doi:10.1016/j.jastp.2008.07.015] a complete seasonal study of the micrometeor input function (MIF) at high latitudes using meteor head-echo radar observations performed with the Poker Flat Incoherent Scatter Radar (PFISR). This flux is responsible for a number of atmospheric phenomena; for example, it could be the source of meteoric smoke that is thought to act as condensation nuclei in the formation of ice particles in the polar mesosphere. The observations presented here were performed for full 24-h periods near the summer and winter solstices and spring and autumn equinoxes, times at which the seasonal variability of the MIF is predicted to be large at high latitudes [Janches, D., Heinselman, C.J., Chau, J.L., Chandran, A., Woodman, R., 2006. Modeling of the micrometeor input function in the upper atmosphere observed by High Power and Large Aperture Radars, *JGR*, 11, A07317, doi:10.1029/2006JA011628]. Precise altitude and radar instantaneous line-of-sight (radial) Doppler velocity information are obtained for each of the hundreds of events detected every day. We show that meteor rates, altitude, and radial velocity distributions have a large seasonal dependence. This seasonal variability can be explained by a change in the relative location of the meteoroid sources with respect to the observer. Our results show that the meteor flux into the upper atmosphere is strongly anisotropic and its characteristics must be accounted for when including this flux into models attempting to explain related aeronomical phenomena. In addition, the measured acceleration and received signal strength distribution do not seem to depend on season; which may suggest that these observed quantities do not have a strong dependence on entry angle.

© 2008 Elsevier Ltd. All rights reserved.

1. Introduction

The sporadic meteoric flux into the upper atmosphere from sub-millimeter particles in the mass range of 10^{-11} – 10^{-4} g is the source of meteoric metals that are responsible for a number of aeronomical phenomena (Williams and Murad, 2002; Plane, 2003). At polar latitudes, these include noctilucent clouds (NLCs) and polar mesospheric summer echoes (PMSE). These are believed to be formed from meteoric smoke particles acting as the condensation nuclei (CN) for the formation of ice particles (e.g., von Zahn et al., 2002). In order to relate this flux with these phenomena we must understand quantitatively when, where, and how much of this flux occurs in the upper atmosphere. At polar latitudes in particular, modeling efforts as well as radar measurements show that the seasonal variability of the flux is

large (Janches et al., 2004, 2006; Singer et al., 2004; Fentzke et al., 2008). We therefore present in this work the first complete seasonal study of the meteor flux utilizing a high power and large aperture (HPLA) radar in the polar mesosphere/lower thermosphere (MLT) region. We performed meteor head-echo radar observations using the 450-MHz Advanced Modular Incoherent Scatter Radar (PFISR), located at the Poker Flat Research Range (65.126N, 147.495W) near Fairbanks, Alaska. The observations were carried out for ~24-h periods near the summer and winter solstices and spring and autumn equinoxes and were designed to study the diurnal and seasonal characteristics of the meteoric flux at this geographical location. We provide a summary of the data processing algorithms and searching meteor criteria in Section 2. The observed results, which are presented in Section 3, include the diurnal and seasonal variability of the observed meteor rate as well as distributions of the altitude, radial velocity, deceleration, and signal-to-noise ratio (SNR) for the four seasons. In addition, estimates of the meteor dynamical masses are also presented for those events which show deceleration and compared with

* Corresponding author.

E-mail address: diego@cora.nwra.com (D. Janches).

estimates derived in the past using the Arecibo 430-MHz radar (Janches et al., 2000b). Both radars transmit at similar frequencies and thus mass range detection sensitivity issues can be drawn for this comparison, which are independent of plasma frequency issues (Close et al., 2005; Janches et al., 2008; Dyrud et al., 2007a, b). Comparison of the observed results presented here with a model recently developed of the MIF (Janches et al., 2006; Fentzke and Janches, 2008) are presented in a companion paper reported by Fentzke et al. (2008).

2. Observations and data analysis

As a HPLA radar, PFISR detects meteor head-echoes. A meteor head-echo is the radar signal scattered back from a cloud of electrons around a meteoroid moving at or near its speed (Janches et al., 2000a). The cloud forms when ablated material from the meteoroid ionizes as the consequence of collisions between the meteoroid and air molecules upon atmospheric entry (e.g., Dyrud et al., 2007a). Because the meteor head-echo is a target that moves at a speed near the meteoroid's velocity, its detection can be used to deduce a lot of information about the meteoroid characteristics. For the observations reported in this work, we transmitted a $90\ \mu\text{s}$ uncoded radar pulse with an interpulse period (IPP) of 2 ms and a sampling frequency of $1\ \mu\text{s}$ (150 m altitude resolution). The transmitted power was approximately 1.3 MW and a receiver gate delay of $400\ \mu\text{s}$ was used. This scheme allowed us to probe the $\sim 73\text{--}223\ \text{km}$ altitude range.

2.1. Meteor analysis methodology

Fig. 1 shows an example of an event detected by PFISR on June 18, 2007. The meteor event displayed in Fig. 1a was observed by PFISR for a time interval of $\sim 500\ \text{ms}$ (~ 250 IPPs). The rectangular

shape of the detected meteor is due to the fact we transmitted a square pulse. By following the leading edge of the transmitted pulse return, the point from which we measure the altitude of the event, it can be observed that the meteor travels from an altitude of ~ 98 down to $\sim 80\ \text{km}$ during the time it was observed. This translates into a downward motion of $\sim 18\ \text{km}$ in approximately 500 ms giving a first guess radial velocity equal to $\sim 36\ \text{km/s}$. The downward velocity is in excess of the escape speed of the earth indicating that the detected target is of extraterrestrial origin.

To obtain the altitude of a meteor, we convolve a square pulse, which is the nominal transmitted power with the recorded power from the returned pulse. The returned complex voltages and power of the meteor in Fig. 1a for the 130th IPP can be seen in Fig. 1b and c. If a meteor is present in a given IPP this matched-filtering operation results in a triangular-like shape, which is the product of convolving two rectangular signals as shown in Fig. 2. Because we choose to measure the meteor altitude from the leading edge of the pulse and the maximum of the convolution is located at the midpoint, the altitude of the meteor is derived by subtracting 6.75 km (i.e. half of the pulse coverage; $90\ \mu\text{s} = 13.5\ \text{km}$) from the altitude where the convolution peaks.

In order to obtain the instantaneous radial (line-of-sight) velocity of the detected meteor we take advantage of the fact that we can record the complex voltage pairs of each returned sample shown in Fig. 1b. We measure the phase difference in the complex returned voltages (Fig. 1b), which is a product of the Doppler shifted signal from a moving target, by performing an FFT on the returned signal. This calculation is shown in Fig. 3 where the velocity spectra of the voltages displayed in Fig. 1b is shown. It can be observed in this figure that a sharp peak occurs at $37.4\ \text{km/s}$ in agreement with the first guess estimate obtained using the meteor total time and altitude span. The velocity estimates from the least-squared fitting routine of the Gaussian curves results in values with errors of the order of $\sim 0.2\ \text{km/s}$.

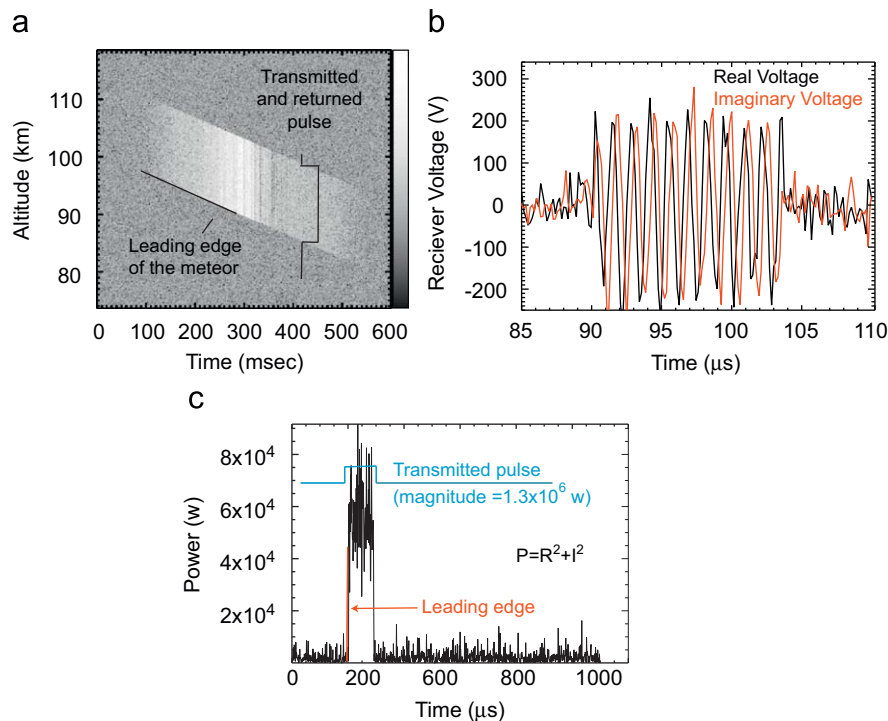


Fig. 1. (a) Range-time-intensity (RTI) image of the received power where a meteor event is present. Each vertical row in this image corresponds to one IPP. The rectangular shape is due to the $90\ \mu\text{s}$ uncoded radar pulse. (b) The received voltage samples for a single IPP where a meteor event is present. The almost constant wavelength sinusoidal shape of the signal is due to the detection of a moving target. The distinct phase difference between the real and imaginary voltage components is product of the Doppler shift. (c) Recorded returned power for a single IPP of the event shown in panel a. The returned power exhibits the same square shape as the transmitted uncoded pulse. The leading edge of the meteor represents the first detection and corresponds to the altitude of the meteor.

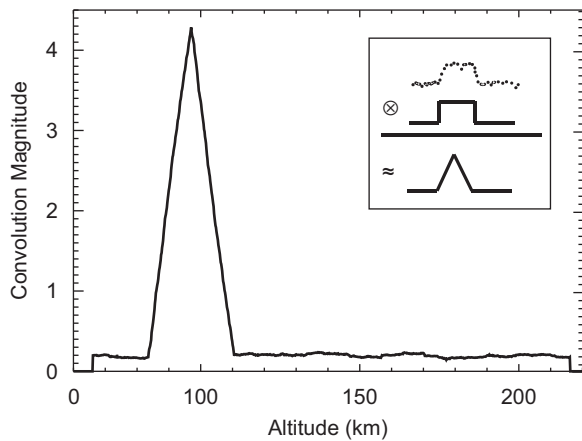


Fig. 2. Convolution between the detected and transmitted pulse for the same IPP shown in Fig. 1b.

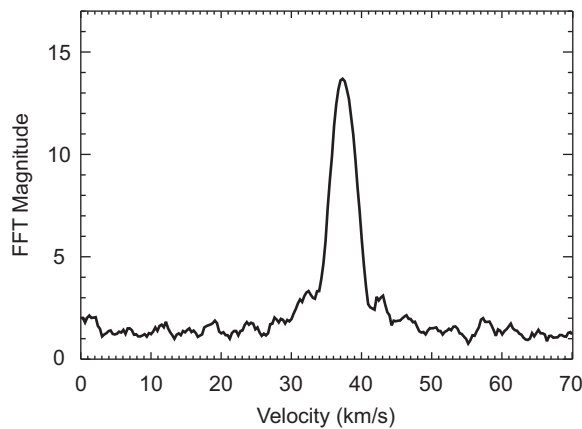


Fig. 3. FFT of a single IPP of the event shown in Fig. 1a. The frequency of the resulting spectra is converted into velocity in km/s. For this particular IPP the speed of the meteor results in ~ 36 km/s.

By repeating the calculation of the meteor altitude and velocity for every IPP where the meteor is present we can determine the time evolution of the meteor height and velocity during the interval for which it is detected by PFISR as displayed in Fig. 4 (panels a and b). The error in the altitude estimates is ± 75 m since our sampling rate of $1 \mu\text{s}$ limits us to an altitude resolution of 150 m. Note that in Fig. 4b the meteor velocity decreases as the meteor travels through the radar beam allowing us to measure precise meteor deceleration. Finally, an estimate of the returned signal strength can be obtained by calculating the meteor SNR shown in Fig. 4c. In particular, the SNR displayed in Fig. 4c shows a significant temporal variability on its strength. Kero et al. (2005) and Mathews et al. (2007) suggested that these SNR modulations may indicate the detection of multiple bodies produced by a fragmenting event. The particular meteor events studied by these authors show a pronounced periodicity in the SNR fluctuations. Recently, Dyrud et al. (2007b) reported a plasma simulation of radio waves reflected from the meteor head-echo and showed that if the peak plasma frequency is close to the radar frequency, the scattering will occur in the Mie regime and thus show destructive and constructive interference patterns. The lack of periodicity in the SNR shown in Fig. 4c suggests that the modulation for this particular case may be caused by these plasma interference patterns rather than fragmentation. This is supported by the smoothness of the Doppler profile shown in Fig. 4b.

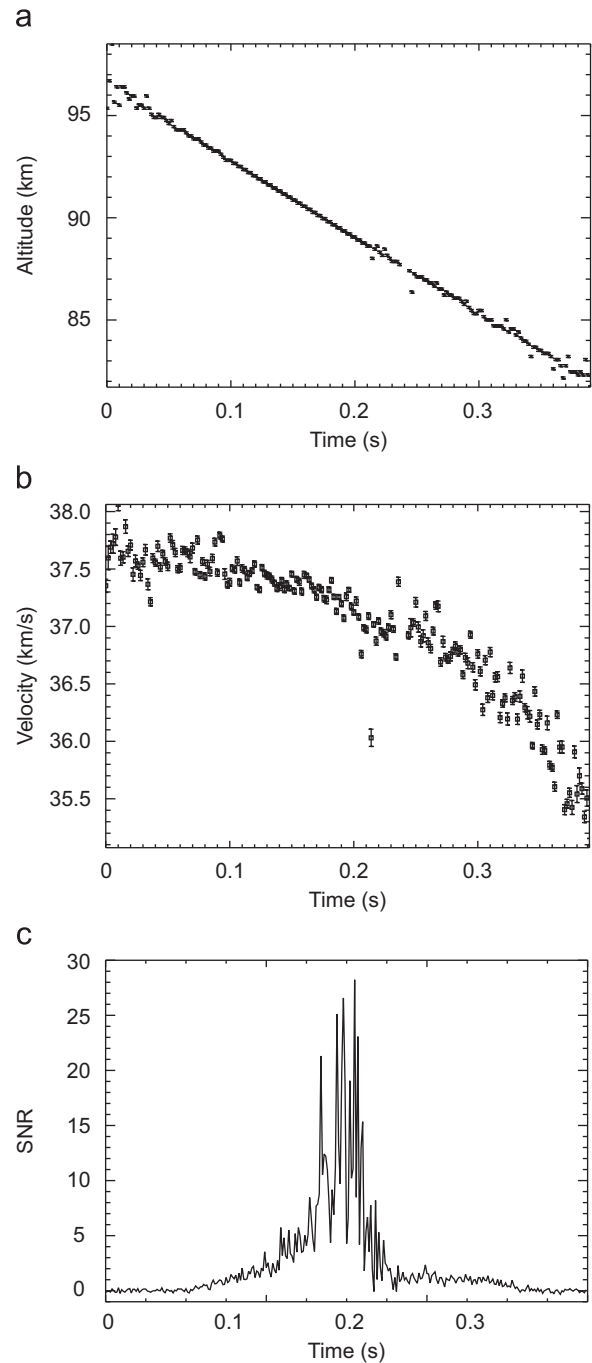


Fig. 4. Observed parameters as a function of time for the meteor event presented in Fig. 1 (a) Altitude-Error bars include ± 75 m due to the sampling rate of $1 \mu\text{s}$ (150 m). (b) Line-of-sight-error bars include the 1-sigma error estimate for the peak of the Gaussian curve fitted to the velocity spectra shown in Fig. 3. (c) SNR.

2.2. Meteor searching algorithm

We have developed an automated searching routine that utilizes the previously discussed signature analysis to find and characterize all the detected meteor events during our observations. Our searching methodology is based on identifying peaks in the frequency space in each IPP, which are above a pre-defined threshold. This threshold is defined by performing a running noise characterization through the entire data set. The process is summarized in Fig. 5. We determined that, peaks with values equal to 6.375σ above the average noise level allows us to detect meteors very close to the noise floor. Once we have defined the

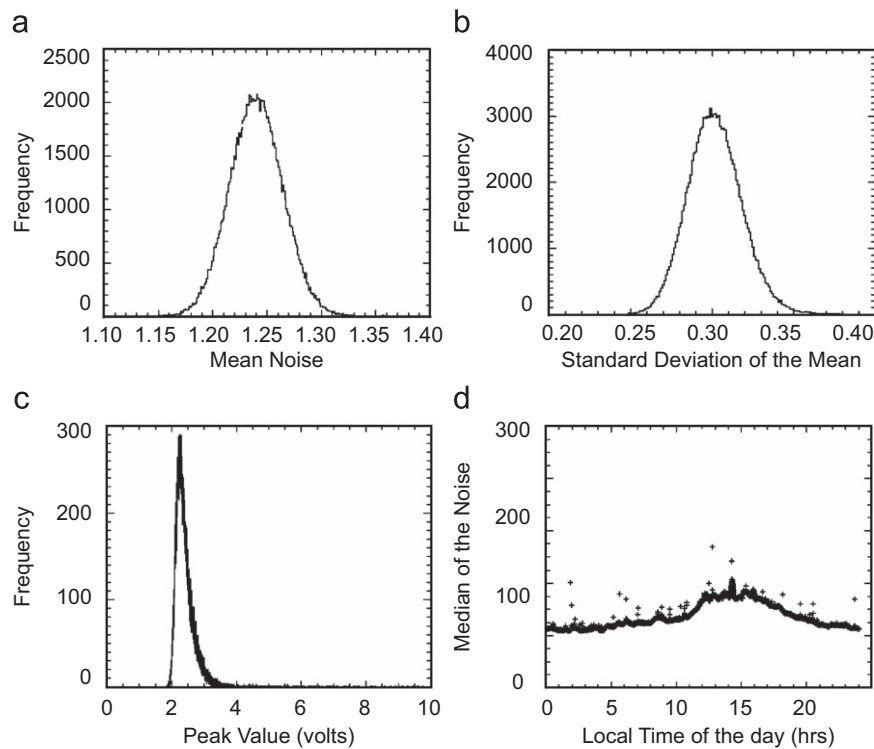


Fig. 5. (a) A histogram of the mean value from the FFT of single IPP's for 5 min of data. (b) Upper left: A histogram of the standard deviation of the mean value of the FFT of single IPP for 5 min of data. (c) Lower left: A histogram of the peak value from the FFT of single IPP's for 5 min of data. (d) Lower right: This is the mean of the mean (peak of Fig. 5a) every 5 min for a full 24 h day. This figure shows the noise floor is dependent on time and thus the threshold must be recalculated continuously.

threshold, we search through the data for events that have at least seven consecutive IPPs with peaks in the velocity spectra satisfying the condition described above. We then calculate the altitude and velocity profiles as a function of time and reject events that are discontinuous. We define discontinuous as a consistent change in height and/or velocity between consecutive IPPs larger than pre-defined values. We also removed events that show upward motion or downward velocities < 1.5 km/s. These slow or altitude increasing events are returns that are characteristic of returns from satellites or Earth orbiting space debris.

We also performed a visual check of a large portion of the recorded events to ensure the fidelity of the results and prevent the introduction of false counts to the resulting statistics. This guarantees that each count we consider is a meteor event and not the result of noise, interference, or satellite returns. Because of the manual checks, one of the only other possible source of error is events being missed by the searching routine. For the March observations, we searched a portion of the data by looking at range-time-intensity (RTI) images of each record (2500 IPPs) similar to Fig. 1a and compared the meteors we found by this method with those found using the searching routine. This analysis showed that the number of missed counts is negligible when compared to the total number of events found with the automated algorithm (about 1% is the estimate of the number of missed meteors). In addition, it was found that the searching algorithm did not favor any distribution of the velocity, time of the day, mass, or acceleration distributions.

3. Results and discussion

We have performed meteor observations covering ~ 24 -h intervals during 4 days, each one characteristic of a different season. The purpose of this observing program is to study the

variability of the meteoric flux as a function of season. The variability of the flux at MLT altitudes is predicted to be larger at polar latitudes than latitudes near the equator (Janches et al., 2004, 2006; Singer et al., 2004). The high dependence on latitude is due mainly to the relative location of the meteoroid sources with respect to the local zenith. At different seasons, sources may lie below the horizon and therefore the Earth will mask a portion the flux. A companion paper by Fentzke et al. (2008) compares a recently develop model of the MIF (Janches et al., 2006; Fentzke and Janches, 2008) with these observations. Table 1 shows the list of observations presented in this work.

3.1. Seasonal variability of the meteor radial velocity distribution

Fig. 6 displays the radial (i.e. line-of-sight) Doppler meteor velocity distributions for the four seasons. Because PFISR does not currently have an interferometry capability, the line-of-sight velocity is the only component that can be measured. Additionally because PFISR's radar beam was pointed vertically for these measurements, the radial component of the velocity is also the vertical component. Referring to Fig. 6, it is evident that the radial meteor velocity distribution is strongly dependent on season reaching a maximum during the fall while the minimum occurs in the spring. The change in the radial velocity distribution from season to season is due to the fact that most of the sporadic meteoroids originate from six known orbital families or sources (Jones and Brown, 1993; Taylor, 1997; Taylor and Elford, 1998). The relative angles between the location of these sources, in the local sky, and the radar beam axis is strongly dependent on season. The average elevation angle of the meteor trajectories is therefore highly dependent upon the time of the year, similarly to the change of the sun's elevation in the sky at high latitudes from season to season. In the springtime, the elevation angle of the average origin of the meteors will be much lower than in the fall.

Table 1
Summary of the results

Season	Observation date	Average velocity (km/s)	Average mass (μg)	Average altitude (km)	Average acceleration (km/s^2)
Spring	March 6, 2007	19.1 ± 0.2	0.0019 ± 0.0005	96.2 ± 0.3	-14.4 ± 0.5
Summer	June 18, 2007	25.1 ± 0.3	0.016 ± 0.002	95.1 ± 0.2	-21.6 ± 0.5
Fall	^a September, 2007	35.1 ± 0.3	0.0087 ± 0.0009	99.2 ± 0.1	-23.8 ± 0.4
Winter	November 30, 2007	31.0 ± 0.3	0.0024 ± 0.0002	100 ± 0.1	-25.5 ± 0.4
Season	Observation date	Average SNR (dB)	Average duration (s)	Time of day for minimum counts (h, AKST)	Time of day for maximum counts (h)
Spring	March 6, 2007	-1.5 ± 0.5	0.059 ± 0.003	18.7	5.8
Summer	June 18, 2007	-1.7 ± 0.4	0.047 ± 0.002	18.8	5.6
Fall	^a September, 2007	-2.0 ± 0.4	0.046 ± 0.002	18.1	6.4
Winter	November 30, 2007	-1.5 ± 0.4	0.0430 ± 0.0002	17.6	6.5

The average values reported here are estimates of the peaks in the corresponding distributions shown in Section 3. Error estimates are given by $\sigma/N^{1/2}$, where σ is the standard deviation and N is the number of points. Note that the values reported in this table are mean values of generally broad distributions provided for comparison purposes. Time of day is presented in local time and does not include daylight savings time.

^a The September data was taken in intervals over the course of three days: September 9, 10, and 14; 2007.

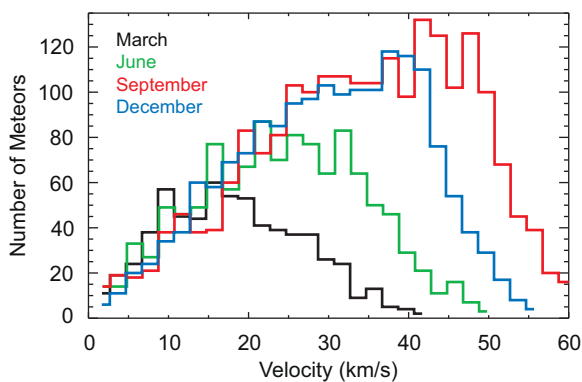


Fig. 6. Observed radial velocity distributions for all the observed seasons.

This translates into a larger vertical component of the meteor velocity in autumn as the observations show. The seasonal variability of the meteor velocity distribution due to the tilt of the Earth with respect to the ecliptic plane has been successfully modeled from measurements taken at Arecibo observatory in Puerto Rico (Fentzke and Janches, 2008) and for the distributions presented here (Fentzke et al., 2008). The spread in the velocity distributions are also in agreement with the observed latitudinal and longitudinal, in the ecliptic frame of reference, width of the sources. In addition, note that the distributions have a significant number of events with speeds below the Earth's escape velocity (11.2 km/s). These events can be due to several factors including: meteors with a large horizontal and a small vertical velocity component, space debris that are de-orbiting, and/or aerocaptured meteors (meteors that are in orbit of a body other than the Earth and glance off of the Earth's atmosphere). Unfortunately none of these can be distinguished from the detected meteors with the current measurement capabilities.

3.2. Diurnal and seasonal variability of the meteor rate

Fig. 7a shows the number of detected meteors per hour as a function of the time of day for a 24-h observing period and the four seasons for which we performed observations. As can be seen in this figure, the diurnal behavior of the meteor rate is independent of season with a minimum occurring at around 1830 AKST and a maximum around 0530 AKST. As predicted by Janches et al. (2006), the seasonal variability of the meteoric rate

at these latitudes observed by HPLA radars is large, with a minimum in spring and a maximum in autumn. Similar but less pronounced variability has been measured at lower latitudes (Dyrud et al., 2005; Janches and Chau, 2005; Janches et al., 2006; Fentzke and Janches, 2008). However, in the polar MLT the flux during spring equinox is only about 30% of that detected during autumn, increasing to about 50% during the summer and winter solstices. This can also be seen in Fig. 7b, where the percentage of detected meteors with respect to the total detections in all the seasons is displayed. This variability agrees with modeled predictions (Fentzke et al., 2008).

Regarding the panels in Fig. 7, lower counts are once again the product of the meteor source locations being lower in the local sky. When the center of the source is low in the sky, at least a portion of the meteor radiants of the particular source will be below the local horizon. This produces the diurnal variability of the meteor rate distribution showing the sources are rising and setting in the local sky. This also produces the seasonal variability since in the spring time at high latitudes, at least a portion of the meteoroid populations are below the horizon. Thus there is less meteoric activity in the MLT in spring than in autumn. In addition and due to the fact that we only measure the vertical component of the velocity we expect to see a cyclic behavior in the radial velocity that mirrors the diurnal and seasonal variabilities (Janches et al., 2003). This effect is shown in Fig. 8 where the average detected radial velocity as a function of time of the day is shown for all the seasons. The highest daily line-of-sight velocities are measured at the same time that the peak of the meteor rate distribution occurs. This peak indicates that this is the time when the radiant of the dominant sources are highest in the local sky. In the same manner, the highest annual radial velocity is measured in fall, when the sources that contribute most of the observed particles reach the highest elevation in the local sky. The study presented here shows that at high latitudes the variability of measured meteor parameters is strongly dependent on season while at lower latitudes this dependence is less pronounced (Janches et al., 2006). The results suggest that most of the observed meteors must originate from sources located around the ecliptic plane.

3.3. Seasonal variability of the meteor altitude distribution

Fig. 9 displays the altitude distribution observed with PFISR for all seasons studied. The altitudes presented in this figure represent the average height from where the meteor head-echo

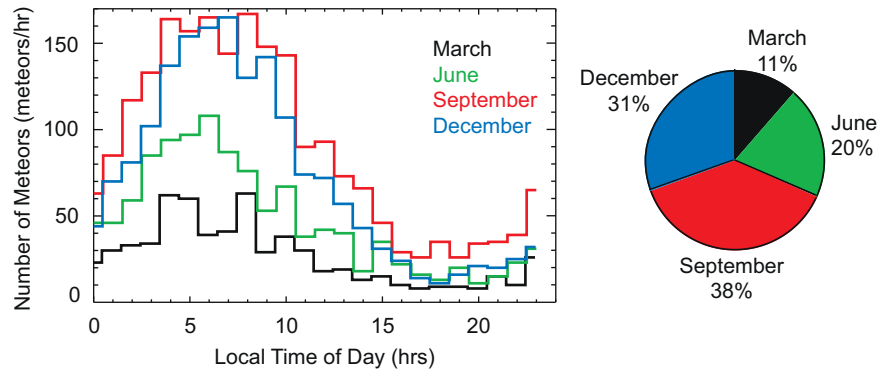


Fig. 7. (a) Observed number of meteors per hour for the four seasons. (b) Percentage of meteors observed during each 24 h observing period relative to the total observed in all the observations.

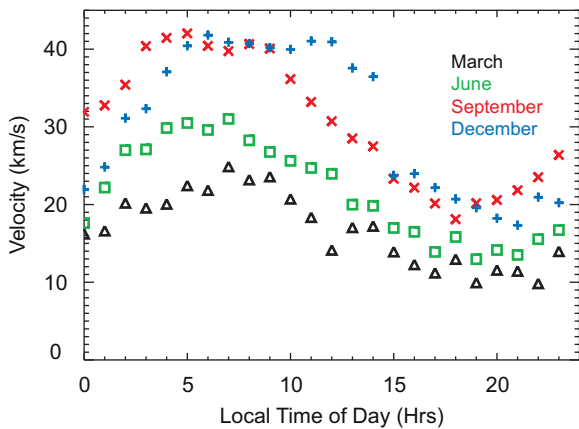


Fig. 8. Average meteoroid velocity as a function of the time of day.

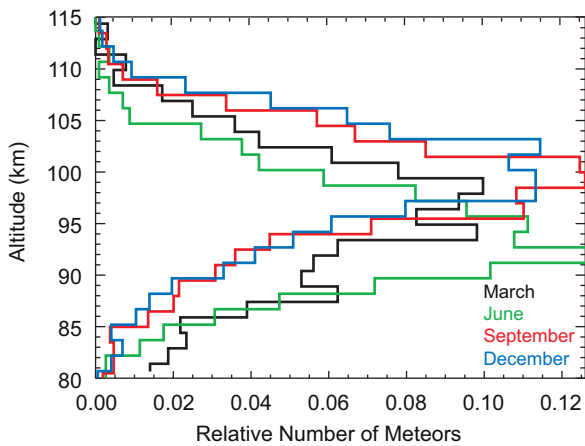


Fig. 9. Observed meteor initial altitude distributions for all the observed seasons.

return is recorded (Janches and ReVelle, 2005). Referring to Fig. 9, we can observe once again a significant seasonal variability of the meteor head-echo altitude distribution observed by PFISR. The distribution peaks at 96.6 km in spring, decreases down to 93.8 km in summer, increases to a maximum of 99.1 km during fall, and peaks at 99.9 km in winter. This variability is much larger than the errors of these estimates, presented in Table 1, indicating that this is a real seasonal change of the ablation profile of meteoroids. In general, the altitude distribution of meteor head-

echoes is a diagnostic of the detection response function of the HPLA radar being used and it will depend on its frequency (Westman et al., 2004; Janches et al., 2008). It is natural then to compare the PFISR observed results with those obtained using, for example, the Arecibo radar, which utilizes a similar frequency (Janches et al., 2003). By performing such a comparison, two differences are immediately obvious. The first difference is that, depending on season, the PFISR distributions are 6–12 km lower than those resulting from the Arecibo observations, which peak at about 105 km (Janches et al., 2003). This is easily explained by PFISR’s lower sensitivity, compared to that of Arecibo. This implies that PFISR requires a higher meteor head-echo electron volume density to reach a minimum detectable limit than the one needed by Arecibo (Fentzke and Janches, 2008; Fentzke et al., 2008). This is only possible for particles with higher radar cross-section (RCS), which are likely to be larger particles penetrating deeper into the MLT in order to produce the required amount of electrons before ablating (Janches et al., 2008; Fentzke and Janches, 2008). The second difference is that the PFISR altitude distributions show a significant seasonal variability, which is not present, at least with such intensity, at lower latitudes (Janches et al., 2003). Since the results presented here are obtained using the same instrument, the variability can only be the result of either seasonal differences of the surrounding atmosphere where the meteors are detected or the characteristics of the MIF. Both of these phenomena have large variability at high latitudes and we will show here that both effects play an important role in the resulting altitude differences.

The polar mesopause is known to reach a temperature minimum of ~130 K at ~90 km altitude in summer (Lübken, 1999). This is due to upwelling in the mesosphere accompanying a wave-induced mean meridional circulation driven by gravity wave (GW) drag that closes the mesospheric zonal jet and results in large departures from geostrophic balance (Fritts, 1995). The colder temperatures imply a smaller scale height and lower densities at these altitudes. Thus, with smaller scale height, a given meteoroid will penetrate deeper before evaporating, and since ablated meteor atoms are the source of ionization, the detection will occur at lower altitudes as well (Janches and ReVelle, 2005; Fentzke and Janches, 2008).

The correlation between seasonal variability of the polar mesospheric temperature (and scale height) and the detected meteor altitude have been previously suggested for both meteor trails using a VHF meteor radar at the South Pole (Lau et al., 2006) and head-echoes using the EISCAT VHF/UHF HPLA radar (Westman et al., 2004). In particular, the results reported by Westman et al. (2004) included observations for only two seasons, mid-summer (August) and winter (December), which prevented the determination of additional factors that may cause seasonal

differences in the altitude distribution. Thus while we believe that the minimum altitude observed in June by PFISR is due to lower mesospheric temperatures, there is also a significant difference (~ 2 km) between the distributions observed in spring and autumn/winter that cannot be attributed to changes in atmospheric conditions, as these seasons should be roughly comparable. As shown recently by Janches et al. (2006) and Fentzke and Janches (2008), the directionality of the flux for a given location plays an important role in the manner and the amount of which the flux manifests seasonally in the MLT. This is due to the fact that, as discussed in the previous section, the sporadic meteoroid background originates mostly from very specific radiant distributions (Jones and Brown, 1993; Taylor, 1997). Thus, early in the morning, the time of the day where the influx rate peaks (see Fig. 7), the flux will enter the atmosphere at angles closer to the local zenith in autumn while in spring these angles will be shallower, as discussed in the previous section. This difference causes the marked reduction on the amount of detected events and an increase in the peak of the radial velocity distribution as shown in our observations (Figs. 6 and 7). In terms of the observed altitudes, more vertical entry angle will make meteors detectable at higher altitudes as theoretical calculations show (Janches and ReVelle, 2005; Fentzke and Janches, 2008; Fentzke et al., 2008). Consequently, at higher latitudes and for similar atmospheric conditions, the altitude distribution in autumn should be higher than in spring as the PFISR results presented here show.

3.4. Measured meteor decelerations and dynamical mass distributions

We determine the meteor average deceleration, shown in Fig. 10, by using a linear least squares fit to the velocity profile as a function of time (Fig. 4b). Because the velocity is clearly nonlinear as a function of time we utilize the resulting slope of the linear fit as an average deceleration. However, we are currently developing an algorithm to fit a more appropriate function that will provide more accurate results, similar to the one reported by Bass et al. (2007) but using a robust modeling effort that takes into account the meteor ablation and ionization processes as well as the calculation of the RCS and its radar detection using plasma simulations of electromagnetic waves interacting with the head-echo as it travels through the beam (Dyrud et al., 2007a,b; Dyrud and Janches, 2008). A difference between the observations used by Bass et al. (2007) obtained with the Jicamarca Radio Observatory (JRO) 50 MHz radar in Peru, and those reported here is that unlike JRO, PFISR currently lacks interferometry capabilities. Thus, there is no way to unambiguously determine

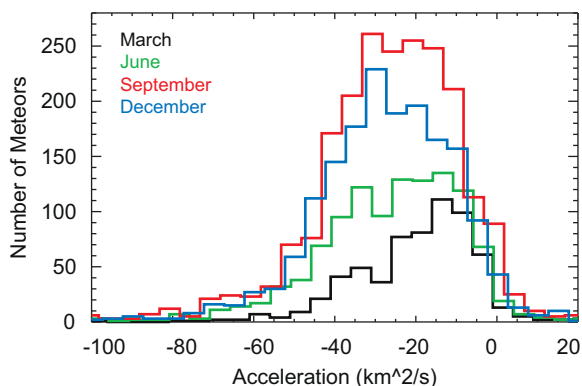


Fig. 10. Meteor deceleration distributions for all the observed seasons.

the location of the meteor within the radar beam. Therefore there is an inherent error in the deceleration measurements introduced by the range reduction of the meteor trajectory while it is being illuminated (Chau and Woodman, 2004). This error depends on the unknown $d\alpha/dt$ term, where α is the angle between the instantaneous location of the meteor and the radar beam axis. For a narrow beam such as the Arecibo radar, this error may be small, but for PFISR and JRO's wider beams this needs to be considered more carefully as shown by Chau and Woodman (2004). We have shown that, on average, the atmospheric entry angle of the meteors with respect to the beam axis changes with season, being generally high in spring and low in autumn giving marked changes in meteor rate, radial velocity, and altitude distributions. However, looking at the results displayed in Fig. 10, there seem to be little dependence of the measured deceleration with seasons, thus suggesting that on average, the $d\alpha/dt$ term may not introduce a large error.

We are now interested in obtaining an average estimate of the meteoroid mass range detectable by PFISR. For this we calculate the dynamical mass using the meteor momentum equation together with the measured altitude, velocity and deceleration and a model atmospheric density (Janches et al., 2000b) given by

$$m \frac{dV}{dt} = -\Gamma \rho_{\text{air}} S V^2 \quad (1)$$

where m is the meteoroid mass, dV/dt is the measured acceleration, Γ is the drag coefficient (1 for this work), S is the cross-sectional area, ρ_{air} is the atmospheric density taken from the MSIS-E-90 atmosphere model (Hedin, 1991) and V is the measured Doppler velocity.

Because we do not know the error introduced by the $d\alpha/dt$ term and given the arguments described above regarding the lack of angle dependence we ignore it at this stage. However, an attempt to estimate this error is presented in Section 3.5. Fig. 11 shows the meteoroid dynamical mass distribution for all the seasons calculated using Eq. (1). We assume for this calculation a meteoroid mass bulk density of 3 g/cm^3 . It can be observed from this figure that the distributions peak at mass value equal to of $\sim 0.7 \times 10^{-2} \mu\text{g}$, which is about 1–2 orders of magnitude larger than those derived using the more sensitive Arecibo radar (Janches et al., 2000b, 2008; Mathews et al., 2001; Fentzke et al., 2008). This is in agreement with the altitude differences between the height distributions observed by both radars as discussed earlier in Section 3.3. The fact that the PFISR altitude distributions peak significantly lower than those measured at Arecibo indicates that

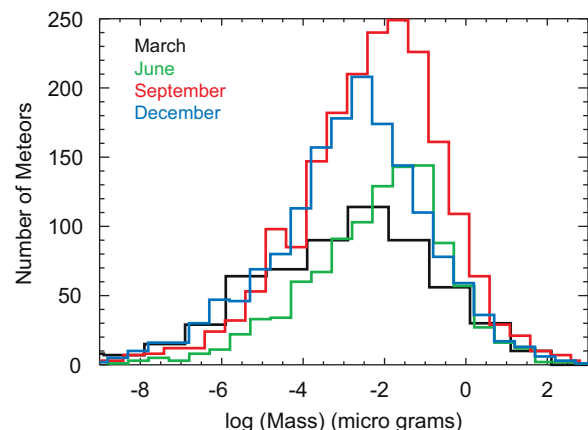


Fig. 11. Meteoroid dynamical mass distributions and for all the observed seasons.

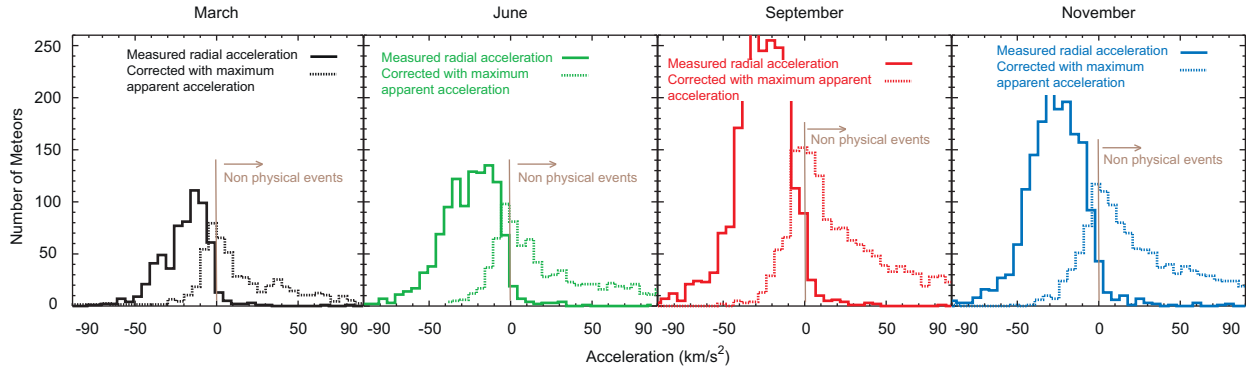


Fig. 12. Corrected and Uncorrected meteor deceleration distributions for all the seasons studied. The corrected distributions assume the maximum possible range reduction apparent acceleration as described in the text.

this less sensitive radar detects more massive particles. One important point to note is that the reason why Arecibo may not efficiently detect the heavier particles that PFISR seems to detect is due to the differences in the collecting area. PFISR is less sensitive than Arecibo because of its smaller aperture and larger observing volume. Heavier particles are less frequent (Ceplecha et al., 1998; Mathews et al., 2001), thus a larger volume is needed to consistently detect them.

3.5. Estimation of the apparent acceleration due to target range reduction

The absolute acceleration of a target traveling through a radar beam can be written as (Chau and Woodman, 2004)

$$a \approx a_r + \left(\frac{v_r R_0}{\Delta t \Delta R} \right) \Delta \alpha^2 \quad \text{or} \quad a \approx a_r + c \alpha^2 \quad (2)$$

where the second term on the right hand side of Eq. (2) is an apparent acceleration introduced by the reduction of the instantaneous range of the target while it is being illuminated. As discussed earlier, α is the angle between the instantaneous location of the meteor and the radar beam axis. Thus, $\Delta \alpha / \Delta t$ is the total change of this angle during the time it takes the meteor to cross the radar beam. In addition, v_r is the radial (i.e. vertical in our case) velocity component and ΔR is the range traveled during the interval Δt . As can be seen in Eq. (2), when $\Delta \alpha$ is equal to zero, (i.e. the tangential path across the radar beam is small) the total acceleration is the measured radial acceleration.

Since we have no manner to determine where within the radar beam the meteor was detected at, we must make assumptions in order to estimate how large the apparent acceleration term can be with respect to measured radial deceleration. The maximum $\Delta \alpha$ that a meteor can experience is equal to PFISR’s beam width (i.e. 0.035 rad; 2° considering the first side lobes). Fig. 12 shows a comparison between the measured deceleration and the corrected one assuming $\Delta \alpha$ is maxima for all the seasons (i.e. every meteor travels through the beam center). Regarding Fig. 12, it can be seen that, considering this “worst case” scenario results on more than half of the particles to have positive acceleration which is unphysical. In addition, the distribution peak at 0 km/s², which represents a shift between ~15 and 25 km/s² depending on season. The consistency between seasons and the fact that most of the “corrected” accelerations become unrealistic suggest once again that most of the meteor are detected only through a smaller portion of the radar beam which results on a smaller introduced apparent deceleration. Although we cannot estimate it precisely, these results suggest that on average it must be only a few km/s².

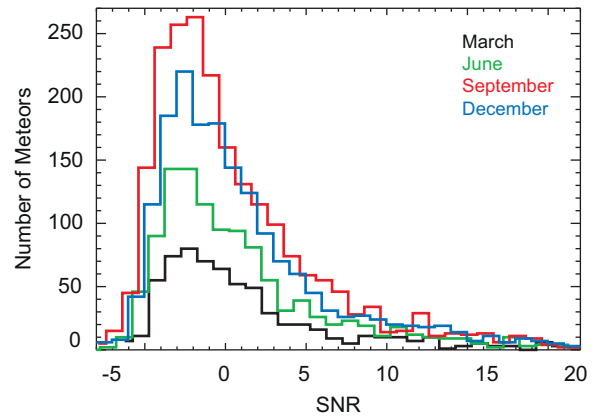


Fig. 13. Average SNR distribution for all the seasons.

3.6. Meteor head-echo SNR distributions

Finally, we present in Fig. 13 the meteor average SNR distribution for all seasons. For a given event, we calculate an average SNR for each IPP. We then average over all the IPPs for the entire duration of the meteor. Referring to Fig. 13 and Table 1, we find that for all seasons the average SNR detected by PFISR is -1.7 dB. The variance of the peak SNR is well within the error bounds and therefore does not appear to depend on season even though it was shown that the entry angle has a strong dependence. This is in agreement with the argument that head-echo phenomena is a spherical target and thus will not be aspect sensitive as polarization measurements reported by Close et al. (2002) have shown. This also is in agreement with simulations presented by Dyrud et al. (2007a, b).

4. Conclusion

We have reported in this manuscript the first complete seasonal study of the meteor flux at high latitudes observed using the 450 MHz Poker Flat Incoherent Scatter radar (PFISR). The results indicate a strong variability in the number of meteors, radial velocity, and altitude distributions for different seasons. All of these results are in agreement with modeling predictions reported by Janches et al. (2006) and Fentzke et al. (2008). The seasonal dependence shows that the micrometeoroid flux into the upper atmosphere is strongly anisotropic. The large seasonal variability was shown to be caused by changes in the location of

the radiant sources in the local sky. During late winter and early spring the radiants are low in the local sky resulting in shallow entry angles (i.e. slow measured radial velocities), which is also manifested by a significant reduction in the number of meteoroids ablating in the polar MLT. The number of meteors increases by a factor of four in late summer and early fall when the meteor sources reach the highest elevations with respect to the local horizon. These observations also show that the altitude distribution peak varies significantly with season reaching a minimum in summer and a maximum in autumn. The minimum altitude occurs at the time when the polar mesosphere is characterized by the lowest temperatures suggesting that smaller scale height and lower densities at these altitudes are responsible for the altitude minimum, and thus the ablated meteoric mass is deposited lower in the MLT. The maximum altitude occurs at the time when the radiants of the major sources are highest in the local sky, hence particles will enter the atmosphere at angles closer to vertical than at other seasons. A given meteor traveling at an angle closer to the local zenith will reach a detectable RCS at a higher altitude than one entering the atmosphere at a shallower angle. Most aeronomical models that utilize meteoric flux contributions to study atmospheric phenomena such as metallic layers, meteor ablation, and PMC formation rarely consider the directionality of the incoming flux and adopt a constant average incoming entry angle as if the sporadic meteoroid radiant distribution is isotropic (McNeil et al., 1998, 2002; Plane, 2004; Megner et al., 2006). These results show that this simple assumption can lead to significant errors as the measured differences can be important when trying to understand, for example, the relation between the MIF and aeronomical processes such as the microphysics involved in the formation of NLCs and PMCs. A difference in the height of maximum ablation of 6 km should be considered when modeling the condensation and nucleation processes that are necessary for the formation of PMSE and NLC. We have also estimated the dynamical mass range to which PFISR is sensitive which is about 2 orders of magnitude larger than the mass range to which the Arecibo 430 MHz radar is sensitive.

Acknowledgements

The PFISR is operated by SRI International under NSF ATM-0608577 cooperative agreement. This work was supported under NSF Grants ATM-05311464 to NWR.

References

- Bass, E., Oppenheim, M., Chau, J.L., Olmstead, A., 2007. Improving the accuracy of meteoroid mass estimates from head echo deceleration. *Earth, Moon, and Planets*, doi:10.1007/s11038-007-9202-2.
- Cepelcha, Z., Boroviccka, J., Elford, W.G., Revelle, D.O., Hawkes, R.L., Porubcan, V., Simek, M., 1998. Meteor phenomena and bodies. *Space Science Review* 84, 327–471.
- Chau, J.L., Woodman, R.F., 2004. Observations of meteor head echoes using the Jicamarca 50 MHz radar in interferometer mode. *Atmospheric Chemistry and Physics* 4, 511–521.
- Close, S., Oppenheim, M., Hunt, S.M., Dyrud, L., 2002. Scattering characteristics of high-resolution meteor head echoes detected at multiple frequencies. *Journal of Geophysical Research* 107 (A10), 1295, doi:10.1029/2002JA009253.
- Close, S., Oppenheim, M., Durand, D., Dyrud, L., 2005. A new method for determining meteoroid mass from head-echo data. *Journal of Geophysical Research* 110, doi:10.1029/2004JA010950/A09308.
- Dyrud, L., Janches, D., 2008. Modeling the meteor head echo using Arecibo radar observations. *Journal of Atmospheric and Solar-Terrestrial Physics*, doi:10.1016/j.jastp.2008.06.016.
- Dyrud, L.P., Denney, K., Urbina, J., Janches, D., Kudeki, E., Franke, S., 2005. The meteor flux: it depends how you look. *Earth, Moon, and Planets*, 95, doi:10.1007/s11038-005-9001-6.
- Dyrud, L., Wilson, D., Boerve, S., Trulsen, J., Pecseli, H., Close, S., Chen, C., Lee, Y., 2007a. Plasma and Electromagnetic Simulations of wave simulations of meteors. *Journal of Advances in Space Research*, doi:10.1016/j.asr.2007.03.048.
- Dyrud, L., Wilson, D., Boerve, S., Trulsen, J., Pecseli, H., Close, S., Chen, C., Lee, Y., 2007b. Plasma and electromagnetic simulations of meteor head echo radar reflections. *Earth, Moon, and Planets*, doi:10.1007/s11038-007-9189-8.
- Fentzke, J.T., Janches, D., 2008. A semi-empirical model of the contribution from sporadic meteoroid sources on the meteor input function observed at Arecibo. *Journal of Geophysical Research (Space Physics)* 113, A03304, doi:10.1029/2007JA012531.
- Fentzke, J.T., Janches, D., Sparks, J.J., 2008. Latitudinal and seasonal variability of the micrometeor input function: A study using model predictions and observations from Arecibo and PFISR. *Journal of Atmospheric and Solar-Terrestrial Physics*, this issue, doi:10.1016/j.jastp.2008.07.015.
- Fritts, D.C., 1995. Gravity wave forcing and effects in the mesosphere and lower thermosphere, pp. 89–+, the upper mesosphere and lower thermosphere: a review of experiment and theory. *Geophysical Monograph* 87.
- Hedin, A.E., 1991. Extension of the MSIS thermospheric Model into the Middle and Lower Atmosphere. *Journal of Geophysical Research* 96, 1159.
- Janches, D., Chau, J.L., 2005. Observed diurnal and seasonal behavior of the micrometeor flux using the Arecibo and Jicamarca radars. *Journal of Atmospheric and Solar-Terrestrial Physics* 67, 1196–1210.
- Janches, D., ReVelle, D.O., 2005. The initial altitude of the micrometeor phenomenon: comparison between Arecibo radar observations and theory. *Journal of Geophysical Research* 110, A08307, doi:10.1029/2005JA011022.
- Janches, D., Mathews, J.D., Meisel, D.D., Getman, V.S., Zhou, Q.-H., 2000a. Doppler studies of near-Antapex UHF radar micrometeors. *Icarus* 143 (2), 347–353.
- Janches, D., Mathews, J.D., Meisel, D.D., Zhou, Q.H., 2000b. Micrometeor observation using the Arecibo 430 MHz radar: I. determination of the ballistic parameter from measured doppler velocity and deceleration results. *Icarus* 145, 53–63.
- Janches, D., Nolan, M.C., Meisel, D.D., Mathews, J.D., Zhou, Q.H., Moser, D.E., 2003. On the geocentric micrometeor velocity distribution. *Journal of Geophysical Research (Space Physics)* 108, 1222, doi:10.1029/2002JA009789.
- Janches, D., Palo, S.E., Lau, E.M., Avery, S.K., Avery, J.P., de la Peña, S., Makarov, N.A., 2004. Diurnal and seasonal variability of the meteoric flux at the South Pole measured with radars. *GRL* 31, L20807, doi:10.1029/2004GL021104.
- Janches, D., Heinselman, C.J., Chau, J.L., Chandran, A., Woodman, R., 2006. Modeling of the micrometeor input function in the upper atmosphere observed by High Power and Large Aperture Radars. *Journal of Geophysical Research* 11, A07317, doi:10.1029/2006JA011628.
- Janches, D., Close, S., Fentzke, J.T., 2008. A comparison of detection sensitivity between ALTAIR and Arecibo meteor observations: can high power and large aperture radars detect low velocity meteor head-echoes. *Icarus* 193, 105–111.
- Jones, J., Brown, P.G., 1993. Sporadic meteor radiant distribution: orbital survey results. *Monthly Notices of the Royal Astronomical Society* 265, 524–532.
- Kero, J., Szasz, C., Pellinen-Wannberg, A., Wannberg, G., Westman, A., 2005. Power fluctuations in meteor head echoes observed with the EISCAT VHF radar. *Earth, Moon, and Planets*, doi:10.1007/s11038-005-3090-0.
- Lau, E.M., Avery, S.K., Avery, J.P., Janches, D., Palo, S.E., Schafer, R., Makarov, N.A., 2006. Statistical characterization of the meteor trail distribution at the South Pole as seen by a VHF interferometric meteor radar. *Radio Science* 41, 4007, doi:10.1029/2005RS003247.
- Lübken, F.-J., 1999. Thermal structure of the arctic summer mesosphere. *Journal of Geophysical Research* 104, 9135–9150.
- Mathews, J.D., Janches, D., Meisel, D.D., Zhou, Q.H., 2001. The micrometeoroid mass flux into the upper atmosphere: Arecibo results and a comparison with prior estimates. *Geophysical Research Letters* 28, 1929–1932.
- Mathews, J.D., Brzinski, S.J., Meisel, D.D., Heinselman, C.J., 2007. Radio and meteor science outcomes from comparisons of meteor radar observations at AMISR poker flat, Sondrestrom, and Arecibo. *Earth, Moon, and Planets*, doi:10.1007/s11038-007-9168-0.
- McNeil, W., Lai, S., Murad, E., 1998. Differential ablation of cosmic dust and implications for the relative abundances of atmospheric metals. *Journal of Geophysical Research* 103 (D9), 10899–10911.
- McNeil, W., M.E., Plane, J., 2002. Models of meteoric metals in the atmosphere. In: Murad, E., Williams, I. (Eds.), *Meteors in the Earth's Atmosphere*. University Press, Cambridge, pp. 265–287.
- Megner, L., Rapp, M., Gumbel, J., 2006. Distribution of meteoric smoke—sensitivity to microphysical properties and atmospheric conditions. *Acp* 6, 4415–4426.
- Plane, J.M.C., 2003. Atmospheric chemistry of meteoric metals. *Chemical Review* 103, 4963–4984.
- Plane, J., 2004. A new time-resolved model for the mesospheric Na layer: constraints on the meteor input function. *Atmospheric Chemistry and Physics* 4, 39–69.
- Singer, W., Weiß, J., von Zahn, U., 2004. Diurnal and annual variation of meteor rates at the Arctic circle. *Atmospheric Chemistry and Physics* 4, 1355–1363.
- Taylor, A.D., 1997. Radiant distribution of meteoroids encountering the Earth. *Advances in Space Science* 20 (8), 1505–1508.
- Taylor, A.D., Elford, W.G., 1998. Meteoroid orbital element distribution at 1 AU deduced from the Harvard Radio Meteor Project observations. *Earth Planets Space* 50, 569–575.
- Westman, A., Wannberg, G., Pellinen-Wannberg, A., 2004. Meteor head echo altitude distributions and the height cutoff effect studied with the EISCAT HPLA UHF and VHF radars. *Annales Geophysicae* 22, 1575–1584.
- Williams, I.P., Murad, E., 2002. *Meteors in the Earth's Atmosphere*. In: Murad, E., Williams, I.P. (Eds.), Cambridge University Press.
- von Zahn, U., Höffner, J., McNeil, W.J., 2002. Meteor Trails as observed by Lidars. In: Murad, E., Williams, I.P. (Eds.), *Meteors in the Earth's Atmosphere*. Cambridge University Press, Cambridge.